Astron. Astrophys. 128, 384–390 (1983)

ASTRONOMY AND ASTROPHYSICS

The shock-induced variability of the Hα emission profile in Mira*

D. Gillet, E. Maurice, and D. Baade

European Southern Observatory, Karl-Schwarzschild-Strasse 2, D-8046 Garching bei München, Federal Republic of Germany

Received June 6, accepted August 5, 1983

Summary. Observations of the Hα emission profile of Mira at phases between −0.05 and +0.60 are reported. At a resolution of 56 mÅ two real emission components are distinguished, while the apparent number of components is larger due to superimposed variable molecular absorption lines. The second redshifted emission component appears at phase +0.14. A qualitative interpretation in the framework of the spherical shock theory is given. The redshifted emission is explained as due to the shock in the hemisphere opposite the observer. The shock is initially optically thick; it becomes gradually thinner as the phase increases. Comparison of the observations and our interpretation is made with the models of Hinkle et al. (1982) and of Willson et al. (1982).

Key words: Mira stars – individual stars (Mira) – molecular stellar atmosphere – shock wave

I. Introduction

The hydrogen emission lines of Mira (*o* Ceti) are known to have several components. Joy (1947) reported a few microphotometer tracings of Hα and Hγ through H11 at phases before and after the luminosity maximum ($-0.12 \lesssim \phi \lesssim +0.35$). The coudé spectrographs of the 100-inch and 60-inch telescopes (Mount Wilson) were used at dispersions up to 3 Å/mm^{-1}. These observations confirmed earlier results that the number and the intensity of emission components initially increase with phase, but finally disappear completely.

Merrill (1955) recapitulated the intuitive explanation of this phenomenon which was outlined in Joy's (1947) historical review. The disturbance, which causes the emission lines, appears first in the deep atmosphere before the maximum of luminosity. The atoms and molecules above it cause the narrow absorptions within the hydrogen emission lines. Since number and positions of those absorption features are very different for different emission lines, they can only be due to line absorption. With the disturbance moving outward, the column densities of atoms and molecules decrease. Thus the intensity and the number of absorptions decrease with phase. Joy (1947) gives for Mira the identification of absorption lines (TiO and metals) that mutilate the underlying hydrogen emissions. Merrill (1955) proposed that the disturbance of the atmosphere which reveals itself by the emission lines must be due to a shock wave. This idea has been expanded and applied to several Mira stars by a number of authors, e.g., Deutsch and Merrill (1959), Gorbatskii (1961), Meahara (1968), Tsuji (1971), Hinkle and Barnes (1979), Willson (1976), Willson and Hill (1979), Hill and Willson (1979), Wood (1979), and Hinkle et al. (1982).

In this paper we report high-resolution observations of the Hα emission in Mira. Section II is devoted to the observational and reduction techniques used. Section III describes the profiles, and a qualitative interpretation based on shock theory is given in Sect. IV. Section V compares this shock model with other ones proposed in the literature. In the last section we summarize our conclusions.

II. Observations and data reduction

The Coudé Echelle Spectrometer (CES) of the European Southern Observatory, with a 1870-diode Reticon as detector, was used with the 1.4 m Coudé Auxiliary Telescope (CAT) or the 3.6 m telescope for the observations. The general characteristics of this high resolution spectrometer have been described by Enard (1982). At a mean dispersion of 2.03 Å mm^{-1} around Hα, the spectrum length is 56 Å. The slit limited resolution was 56 mÅ (2.6 km s^{-1}; resolving power $1.2\,10^5$) while each pixel is 30 mÅ wide. Table 1 gives the general characteristics of each spectrum. The signal-to-noise ratio was evaluated for the "continuum" of Mira.

Typically four or five short (~20 s) integrations on a white light source immediately after each observation of Mira were used for the determination of the mean flat field. The variation of the latter before and after the stellar exposure was negligible. A thorium lamp was used for wavelength calibration. The dispersion curve was determined with high accuracy (twenty thorium lines; rms ≦ 3 mÅ). All these operations were performed on the ESO Image Handling and Processing (IHAP) system.

The contribution of the earth's motion to the observed radial velocities was calculated with the BARVEL subroutine (Stumpff, 1980). The wavelength scale is measured in the center of mass frame of Mira. The radial velocity of the center of mass was assumed to be the mean velocity ($v_{hel} = +56.9 \pm 0.5$ km s^{-1}) of the SiO, H_2O, and OH masers reported by Pierce et al. (1979).

III. The profiles

Figure 1 shows Hα profiles of Mira between phases $\phi = -0.05$ and +0.60 [phases are counted from the luminosity maximum on

Send offprint requests to: D. Gillet

* Based on observations made at the European Southern Observatory at La Silla, Chile

Table 1. Journal of observations of Mira. The resolution is about two pixels. w_b and w_r are the widths (in km s^{-1}) of blueshifted and redshifted emissions, respectively

phase[a]	m_v[b]	date	U.T. at mid exposure	time (mn) exposure	resolution (mÅ)	S/N[e]	w_b (km/s)	w_r (km/s)
-0.045	2.8	01.07.1982	09:58	10.4[c]	56	~ 500	70	--
+0.009	2.5	19.07.1982	10:18	6.0[c]	56	~ 500	70	--
+0.055	2.7	04.08.1982	08:36	50.0[c]	56	~ 500	70	--
+0.139	3.4	31.08.1982	09:42	15.0[c]	56	~ 500	70	24
+0.227	5.1	29.09.1982	06:23	20.0[c]	56	~ 500	70	24
+0.267	5.4	11.10.1982	06:20	20.0[c]	56	~ 500	70	24
+0.403	6.8	26.11.1982	05:21	9.0[d]	~ 66	60	60	26
+0.561	8.6	17.01.1983	01:32	41.7[c]	66	15	50	26
+0.564	8.6	18.01.1983	01:02	45.0[c]	66	15	50	26
+0.603	8.8	31.01.1983	00:55	42.9[c]	66	10	50	26

[a]period: 33od. [b]AFOEV-GEOS [c]telescope: 1.4m [d]telescope: 3.6m [e]at the "continuum"

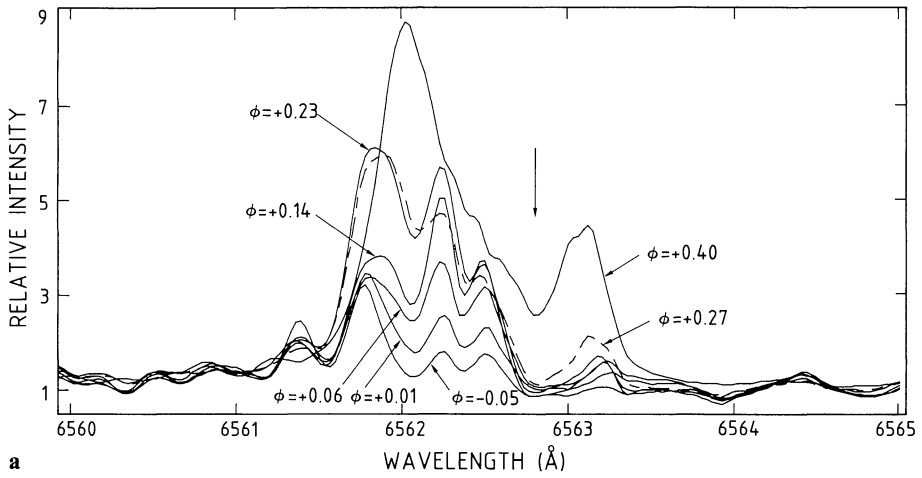

Fig. 1a. Hα profile of Mira between phases −0.05 to +0.40 (see Table 1). The wavelengths are measured in the rest frame of Mira. The relative intensity refers to the mean level of the "continuum" between 6564 Å and 6572 Å. The wavelength of Hα at zero velocity in Mira's rest frame is arrowed. (See text for discussion)

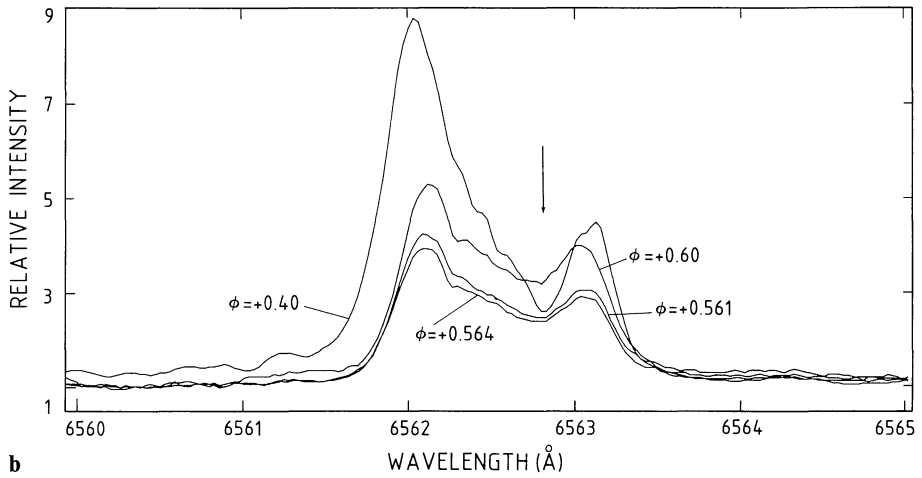

Fig. 1b. Hα profile of Mira between phases +0.40 to +0.60 (see Table 1). The wavelengths are measured in the rest frame of Mira. The relative intensity refers to the mean level of the "continuum" between 6564 Å and 6572 Å. The wavelength of Hα at zero velocity in Mira's rest frame is arrowed. (See text for discussion)

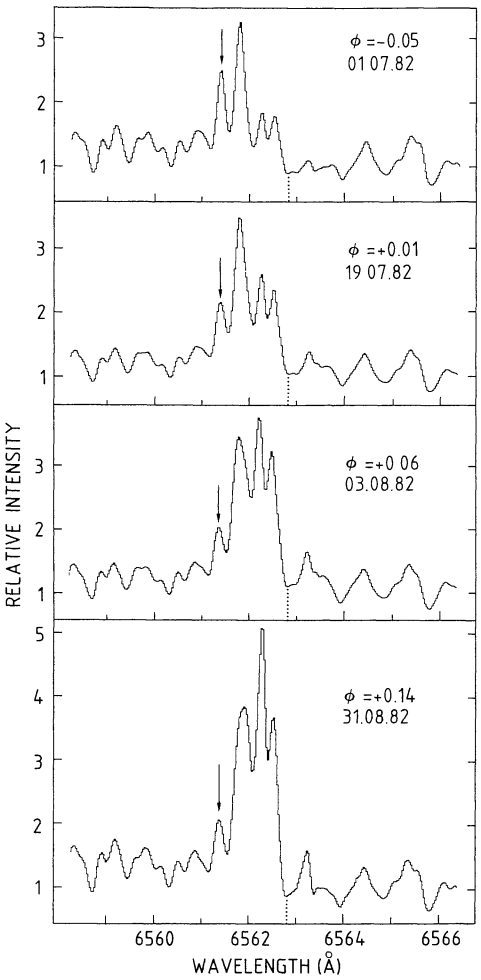

Fig. 2. Evolution of the bluemost component at 6561.4 Å (arrow). At phase −0.05, it has the second highest intensity of all components. In this presentation the individual pixels are visible, each pixel being 30 mÅ wide

JD 2445166.5 (AAVSO) assuming a period of 330 d]. In this cool star it is impossible to determine the continuum with good accuracy. Therefore, the mean intensity of the spectrum between 6564 Å and 6572 Å was normalized to one. This region has no large absorptions or important intensity variations during the cycle. Our observations do not permit an absolute flux calibration, and thus the *Y*-axis measures the combined relative variations of continuum and Hα emission.

1. Description of the blueshifted emission

Figure 1a shows 4 apparent emission components blueward of the rest wavelength of Hα (arrowed). The intensity of the bluemost of these (Fig. 2) behaves like one of the absorptions in the continuum when phase changes from +0.01 to +0.40. But at phase −0.05, its intensity is larger than that of the two least blueshifted components. The three blueshifted absorptions are always present until phase $\phi = +0.23$. Their wavelengths are approximately 6561.6 Å (width ~0.2 Å), 6562.0 Å (width ~0.2 Å), and 6562.4 Å (width ~0.15 Å). Joy (1947) did not find an identification, but Merrill (1960) suggested the TiO molecule. Table 2 gives the lines (γ-system) from the TiO comprehensive Berkeley Listing (Phillips, 1983) that could appear at the position of the observed Hα emission. An identification of the two features is not obvious. A large number of molecular absorptions (TiO, H_2 and other molecules) can occur within the entire Hα profile.

2. Description of the redshifted emission

An other emission, but redshifted, occurs for the first time near phase $\phi = +0.14$. At $\phi = +0.40$ this emission is quite prominent. The shape of both emissions is asymmetric, the blue side of the blueshifted emission being steeper than its red side. The intensity of the latter decreases more slowly. The shape of the redshifted emission is a mirror image of the blueshifted emission, with a steeper red than blue side. These characteristics are clearly seen on the spectrum at $\phi = +0.40$ (Fig. 1a).

3. Comparison of the blue and redshifted emission

The full width of the total blueshifted emission measured at the position of the quasi-continuum (see Fig. 1 and Table 1) decreases from $w_b = 70\,\mathrm{km\,s^{-1}}$ ($\phi = -0.05$) to $w_b = 50\,\mathrm{km\,s^{-1}}$ ($\phi = +0.60$). The width of the redshifted emission increases from $w_r = 24\,\mathrm{km\,s^{-1}}$ ($\phi = +0.14$) to $w_r = 26\,\mathrm{km\,s^{-1}}$ ($\phi = +0.60$).

The relative intensity of blueshifted and redshifted emission (in units of the also variable continuum) increases until $\phi = +0.40$, then declines until $\phi = +0.56$. However, this is not true for the last spectrum $\phi = 0.60$, where both emission lines have become stronger (see Fig. 1b).

Finally (Fig. 1b), the slope of the quasi-continuum bluewards of Hα in the spectrum at $\phi = +0.40$ (or $\phi \leqq +0.40$, see also Fig. 1a) is different from that of the spectra at $\phi \geqq 0.561$.

IV. A qualitative interpretation

In this section, the complex Hα emission profile of Mira and its phase dependent variations are interpreted as the consequence of a spherical shock wave propagation from a point near the photosphere.

Near the maximum luminosity the shock is near the photosphere. This latter occults the receding part of the shock wave (Fig. 3). Consequently, the observer can only see the blueshifted emission produced by the advancing part. Then the large molecular atmosphere gives the absorptions within this emission profile. The interpretation of this first shock phase is developed below in the first subsection. Later, when the front is far from the photosphere, the observer can see the contribution of the receding part of the same shock (Fig. 3). At this moment the absorptions are negligible. This new phase with the problem of the front weakening is discussed in the second subsection. The bluemost blueshifted emission to 6561.6 Å (Fig. 2) is not considered in these two subsections; it will be discussed in the last subsection.

1. The advancing shock phase ($-0.05 \lesssim \phi \lesssim +0.14$)

a) The absorptions

It is assumed that somewhat before the luminosity maximum, an upward shock wave exists in the lower atmosphere of Mira. Initially, the shock moves through the deeper part of the atmo-

Table 2. TiO γ-system lines able to give an absorption within the Hα emission line of Mira (Phillips, 1983). All wavelengths are laboratory wavelengths

λ (Å)	Int.	Band	Rot. line	Vib. band	λ (Å)	Int.	Band	Rot. line	Vib. band
6561.379	13	(4,2)	Q2	85	6562.242	20	(3,1)	R2	121
6561.501	14	(5,3)	P1	20	6562.243	19	(3,1)	Q3	113
6561.542	14	(2,0)	R1	134	6562.245	21	(2,0)	P3	118
6561.665	12	(4,2)	R1	90	6562.373	14	(4,2)	Q1	75
6561.669	12	(4,2)	P3	81	6562.500	14	(5,3)	P1	21
6561.875	16	(4,2)	Q3	93	6562.509	14	(5,3)	R3	82
6561.877	21	(5,3)	R1	50	6562.683	20	(5,3)	Q3	68
6561.947	19	(5,3)	P3	56	6562.694	9	(3,1)	R1	115
6561.958	19	(5,3)	R2	70	6562.767	15	(2,0)	Q3	130
6561.970	19	(5,3)	Q1	32	6562.904	20	(5,3)	Q1; R1	33; 51
6562.053	17	(5,3)	P2	43	6563.027	14	(2,0)	P1	108
6562.113	13	(3,1)	P2; P3	95; 101	6563.307	12	(4,2)	R3	107
6562.233	26	(5,3)	Q2	55	6563.427	10	(3,1)	P1	88
6562.236	20	(4,2)	P1; P2	62; 73					

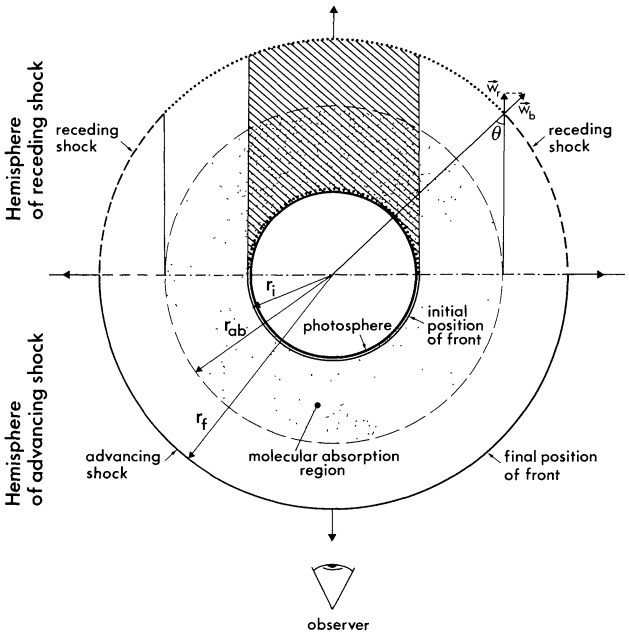

Fig. 3. Schematic diagram of the expanding shock surrounding the photosphere (at Hα wavelength). When the shock is near the photosphere (position *i*), the emission from the receding part of the shock is blocked from view (hatched) by the stellar disk, and cannot be seen by an external observer. The higher density part of the molecular atmosphere initially also blocks (dotted section of the receding shock front) this redshifted emission. It becomes progressively visible (dashed) when the shock radius increases to r_{ab}

sphere (Fig. 3). The emission line is produced in the de-excitation zone behind the front. Without molecules and dust, the Hα photon mean free path is larger than the thickness of the atmosphere because the gas is cool $T<5000$ K). However, there are two main absorptions at 6562.0 Å and 6562.4 Å. The molecules located between the shock front and the upper boundary of the atmosphere absorb part of the Hα photons. The higher the shock, the smaller are the molecule column densities above the shock and, thus, the weaker are these absorptions (viz. Fig. 1a).

b) The blueshifted asymmetric profile

It is possible to understand the asymmetric shape of this profile as due to an optically thick shock in the Hα line. A maximum shock radius R_α of $3\,10^{14}$ cm (see Sect. IV. 2c), an Hα line luminosity L_α of 10^{32} erg s^{-1} ($T_{\rm eff}\sim 2000$ K, distance ~ 60 pc, phase $+0.40$) and an upper limit of $4\,10^4$ K for the temperature in the recombination zone are in fact consistent with a thick shock: $L_\alpha/\pi R_\alpha^2 B(\mathrm{H}\alpha)\gg 1$. Thus, the observer only sees photons from nearest slabs of the de-excitation zone. An integration of the shock flux over the one hemisphere of negligible thickness gives the characteristic shape of the profile clearly seen in the blueshifted emission at phase 0.40 (see Wagenblast et al., 1983).

It is not possible to see this characteristic shape in phases smaller than 0.27 because of the superimposed molecular absorption. However, it is reasonable to assume that the shock is also optically thick in these phases.

In stellar shock waves the internal and potential energies of particles increase faster than the translational energy through the ionization and dissociation zone (Zel'dovich and Raizer, 1966). Thus, a velocity gradient can occur through the de-excitation zone. However, its contribution to the shape of the Hα profile is

negligible in the case of a thick shock, where the observer will only see the outer de-excitation zone slabs in which the velocities are high.

c) The front velocity

The maximum velocity of the de-excitation zone can be inferred from the width of the blue emission component $w_b = 60\,\mathrm{km\,s^{-1}}$. This value is actually an upper limit because the continuum level was certainly underestimated in our width estimation (see, for instance, Maehara, 1968, p. 88) and broadening mechanisms also increase the line width (see e.g. Wagenblast et al., 1983). The latter contribution is difficult to derive with accuracy, but its upper limit is certainly less than $20\,\mathrm{km\,s^{-1}}$, assuming that the electron temperature in the de-excitation zone does not exceed $3\,10^4$ K. If v_s is the front velocity and v_0 the velocity of gas above the present shock which had been lifted by the shock of the previous cycle and is now falling back, the conservation of flux of mass yields:

$$v_s = \left(w_b + \frac{v_0}{\eta_e}\right)\frac{\eta_e}{\eta_e - 1},$$

where η_e is the density ratio between the high velocity de-excitation zone and the region in front of the shock. Note that, v_s, w_b, and v_0, in the stellar rest frame, are absolute values. If one takes into account the broadening the value of w_b will be reduced. Thus, with a limit of the infall velocity, v_0, of $30\,\mathrm{km\,s^{-1}}$ (4 to 5 times the sound velocity in the atomic gas of the lower atmosphere), the front velocity will always be less than $90\,\mathrm{km\,s^{-1}}$. This velocity is smaller in the molecular layers of the atmosphere. If $v_0 = 0$ then v_s is only reduced to $80\,\mathrm{km\,s^{-1}}$. Then, as the ratio $\eta_e/(\eta_e - 1)$ tends to unity when the compression ratio increases, the front velocity is never less than w_b. Thus, the value of v_s is certainly between 50 and $90\,\mathrm{km\,s^{-1}}$, and the shock is strong (Mach number ~ 15).

The above argumentation, of course, assumes that the width of Hα is the largest. As we have observed only this line, high resolution observations of other emission lines (e.g., Paschen lines) are necessary in order to check this.

d) The front acceleration

The shock moves through a medium of decreasing density. In this case, an increase in the front velocity is possible (Whitham, 1958). This effect is not strong in Mira, as between phases +0.06 and +0.40 the width of the blueshifted emission increases slightly from $53\,\mathrm{km\,s^{-1}}$ to $60\,\mathrm{km\,s^{-1}}$ (Fig. 1a). Consequently, the main cause of the increased emission intensity from phase +0.06 to +0.40 is the decline of the absorptions. Near the luminosity maximum, the effect of the diminution of the "continuum level" is certainly of only secondary importance.

2. The appearance of the receding part of the shock ($+0.14 \lesssim \phi \lesssim +0.60$)

From phase $\phi = +0.14$ onwards Hα shows a double emission (Fig. 1a), consisting of the previous blueshifted and a new redshifted component. But only at phase $\phi = +0.40$ can one see that the red component is fully developed. This redshifted emission can be interpreted as the result of the appearance of the shock on the far side of the star, opposite the observer. In the following, it will be called the receding shock although it is part of the same spherical shock (see Fig. 3).

a) The redshifted asymmetric emission

The characteristic asymmetric shape is first observed at $\phi = +0.14$. Before this phase a faint emission develops ($\phi = +0.01$ and +0.06) but it does not show this characteristic asymmetry.

It is possible to explain the blueshifted and redshifted emission in terms of only one shock and a simple atmospheric occultation. To this end, it is necessary to assume that until the luminosity maximum the shock is near the photosphere taken at the wavelength of Hα. The shock leaves the photosphere when the Hα emission line is first seen (about phase −0.2; Joy, 1947). Thus, the observer only sees an advancing front (blueshifted emission). When the shock propagates through the molecular part of the atmosphere the receding part of the shock becomes more and more visible to the observer (redshifted emission). It was already noted (Sect. IV. 1a) that the molecular part of the atmosphere causes a strong absorption of the emission of the advancing shock. The corresponding absorption of the emission from the receding shock is at least three times more important, as the light path through the dense parts of the molecular atmosphere is much longer. The high density zones of the molecular atmosphere occult, like the photosphere, the receding shock until about phase zero. Then an initially weak emission develops ($\phi = +0.01$ and $\phi = +0.06$) when the line of sight no longer intersects the densest zones of the molecular atmosphere. When the shock is far above the photosphere, a large part of the receding shock contributes, like the advancing one, to the observed emission. At this moment, the shape of this visible receding shock is well determined and is the mirror image of the advancing one.

The blue wing of the blueshifted emission and the red wing ($\sim 20\,\mathrm{km\,s^{-1}}$ width) of the redshifted emission have quite a similar slope. This is unexpected since the slope of the red wing should be affected by the fact that the molecular absorption zone is very extended. It is therefore possible that other effects, e.g. the broadening mechanisms (which also yield a width of $20\,\mathrm{km\,s^{-1}}$), dominate the shape of the line wings.

The intensity and the width of the redshifted emission are smaller than those of the blueshifted emission because the highest receding velocities are occulted. To this may add the fact that because of the optical high thickness only the inmost slabs of the receding de-excitation zone can be seen, where the velocities are probably lower.

The slope of the inner wings of the blue- and redshifted profiles decreases with increasing phase (Fig. 1b). This is probably due to a decrease in the optical depth of the shock zone when the shock propagates into the upper atmosphere. Hence, the total emission (blueshifted plus redshifted) must tend towards the classical flat-topped profile resulting from optically thin emission (Mihalas, 1978).

If the infall velocity, v_f, is large enough ($v_f \sim w_r \leqq 25\,\mathrm{km\,s^{-1}}$), the infalling gas may contribute to the red emission via two different mechanisms: Firstly, a very strong shock could produce a sufficiently high Lyα and Lyman continuum flux to produce excited hydrogen atoms either directly or through dissociation and ionization of H_2. Only a quantitative calculation can show how strong such a shock would have to be (Mach number 20–30?). Secondly, it would be interesting to know if the ballistic infall of high velocity gas (Mach number 4–5) can create a second shock front. This inward running shock could produce the profile. In both cases, however, one would at one phase or the other see the emission from the receding shock because the original shock runs over 3 photospheric radii if the estimation of Sec. IV. 2c is correct. Since the appearance of the receding shock is reasonably

well described by our model the aforementioned mechanisms are not likely to be the primary sources of the red emission.

b) The weakening and the disappearance of the radiative shock wave

Figure 1b shows a decrease in the relative emission intensity from phase $\phi = +0.40$ to $+0.56$. Since, at the same time, the continuum intensity declined, too, this means that also the absolute emission strength has decreased. The same effect is also visible on the two spectra taken only one day apart (where $\phi = +0.561$ and $\phi = +0.564$). By $\phi = +0.60$, however, the relative emission intensity has become stronger. This implies that during this phase interval the emission has faded more slowly than the continuum.

After phase $\phi = +0.60$, the mechanical restrictions of the CAT did not allow to observe Mira any further. But we may assume that the dissipation of the shock energy increases with the height of the shock in the atmosphere. The width of the blueshifted emission (Table 1) shows that the front velocity decreases slightly from phase +0.40 on. At the same time, the shock Mach number increases with shock altitude. Joy (1947) showed that the emission in Hγ disappears at about phase +0.65. Thus, the Hα emission most certainly vanishes 20–30 d after phase +0.60 when the Mach number is about equal to 15. The weakening of the shock is thus rapid. Perhaps a sudden dust formation due to the decreasing temperature can provoke a large dissipation of the shock energy. The penetration of a circumstellar shell can also result in a fast dissipation of the shock energy. Anyway, other observations after minimum luminosity are necessary to understand this rapid disappearance of the radiative shock wave.

c) The atmosphere radiative shock zone

Joy (1954) reports that Hγ is in emission during 85% of the period. Therefore the shock runs over approximately $1.7\,10^{14}$ cm if one takes a mean velocity of 70 km s^{-1}. The Hα blueshifted emission appears at phase −0.20 (Joy, 1947) and the absorptions within the profile vanish at about phase +0.30 (Fig. 1a). Thus the thickness $\Delta_{ab} \equiv \Delta_{0.3}$ ($r_{ab} - r_i$ in Fig. 2) of the molecular part of the atmosphere is approximately 10^{14} cm. It is possible to obtain a rough value of the photospheric radius r_i at the wavelength of Hα from the profile at phase +0.40. With the simplified assumption that the molecular atmosphere is perfectly opaque for the emission of the receding shock, simple geometric relations yield:

$$r_i \simeq \frac{\Delta_{0.4}\sqrt{1-(w_r/w_b)^2} - \Delta_{ab}}{1-\sqrt{1-(w_r/w_b)^2}},$$

where $\Delta_{0.4} \equiv r_{0.4} - r_i$ is the distance traveled by the front from its initial position r_i to the one of phase +0.40, and w_r and w_b are the widths of the redshifted and blueshifted emission, respectively (broadening mechanisms neglected). One obtains $r_i \sim 10^{14}$ cm $\sim \Delta_{ab}$. This radius represents about 1.5 photospheric radii at 6560 Å determined by Bonneau et al. (1982) through speckle interferometry. The difference is consistent with the uncertainty of the measurements involved. The distance represents also between 0.1% and 10% of the overall radius of the circumstellar dust shells (Rowan-Robinson and Harris, 1983).

3. A possible reaction of the transition zone

It will be notable that the bluemost blueshifted emission at 6561.4 Å is not a part of the shock emission (see Fig. 2 at phase −0.05). However, relative variations of the continuum and the absorption intensity levels just before the maximum luminosity can explain the decreasing intensity of this emission. Its maximum intensity will be a point near the real continuum and it will be produced by the photosphere and the other emission component by the shock wave. But, if this explanation is not correct, i.e., if the bluemost emission is produced by the wake, then it can be understood as a consequence of the reaction of the transition zone.

In a cool star such as Mira, the temperature of the atmosphere ranges typically from 5000 K at large optical depths to 500 K at very low optical depths. Thus, within the atmosphere, the hydrogen changes from the atomic to the molecular state, which implies the existence of a transition region. Its thickness, like that of the atomic state zone, is only a small fraction of the total thickness of the atmosphere. The shock loses its stationary structure when it crosses the transition region. Steady shock models cannot be applied to this region.

Gillet and Lafon (1983) have shown that the molecular state of hydrogen in a stellar atmosphere has considerable influence on all shock structures. The photodissociation in the shock wave radiative precursor and the thermal dissociation in its wake weaken the shock compared to the propagation in an atomic medium.

Consequently, it is possible to understand the bluemost component (6561.4 Å) at phase −0.05 (Fig. 2). Between phases −0.05 and +0.05, when the shock passes through the transition zone, it will lose much of its energy. Thus, its velocity v_s will decrease from less than 100 km s^{-1} ($w_b \simeq 70$ km s^{-1}) in the atomic atmosphere to less than 70 km s^{-1} ($w_b \simeq 53$ km s^{-1}) in the molecular atmosphere. This may explain the observed decrease in the strength of the feature in question between phases −0.05 and +0.05 (see Fig. 2). Observations at greater negative phases are necessary to check this point. In does in any case not affect the other conclusions derived above.

V. Comparison with other models

In the last section we have applied the shock model only to Mira. It is, however, possible that the main characteristics of this model are common to the majority of Mira stars. Here we compare it with two other shock models whose most recent versions were given by Hinkle et al. (1982) and Willson et al. (1982), respectively.

The first model is based on two and five micron IR spectra of nine Miras. The major observational fact is the variation of the total CO column density as a function of phase. In this model, the shock emerges near the luminosity minimum through the infrared continuum layers, and the CO dissociation vanishes near the maximum. The shock velocity is assumed to be larger than 30 km s^{-1}. This single shock model is qualitatively consistent with our model except for the interpretation of the bluemost component (Sect. IV.3). Thus, the infrared observations allow one to analyse the interaction between shock wave and molecular atmosphere and the subsequent hydrodynamic relaxation of the molecular atmosphere. IR spectroscopy can only observe the shock while it is still deep in the atmosphere. Combination of IR data with optical observations (like the ones of this paper) leads to the conclusion that just after the luminosity *minimum*, about between phases +0.6 and +0.7, there are two strong shock waves in the atmosphere: a lower shock observable only in the infrared and an upper shock only visible at the optical wavelengths.

The model of Willson et al. (1982) is based on an analysis of radial velocities of absorption lines at optical wavelengths. They

claim that near the luminosity *maximum*, there are two shocks: a lower, large amplitude shock, also apparent in infrared wavelengths, and an older, upper shock of smaller amplitude. The Balmer emission lines are thought to be produced by the lower shock. Our observations of Mira show that at about the luminosity maximum only one shock, namely near the photosphere (no redshifted emission observed), exists. A second, upper shock in Mira would not produce a Hα redshifted emission. The receding part of this older shock, at a large distance from the photosphere, must give a red emission component for the ions. Therefore, the Willson et al. model can be qualitatively consistent with our model describing the variation of Mira's Hα profile.

VI. Conclusions

We have collected a set of homogeneous high resolution Hα profiles of Mira between the phases of maximum and minimum luminosity. From these observations the velocity of the front and its variation with time could be deduced. The front acceleration is small. It was shown that the receding part of the shock is only visible at $\phi \gtrsim +0.1$. The reason for this phenomenon is that the shock is initially occulted by the photosphere and the molecular atmosphere. Initially the shock is optically thick and gradually becomes thinner as the phase increases. The shock runs over not more than three Hα photospheric radii between phases -0.2 to $+0.7$. The Mach number is approximately constant and large (~ 15) during this phase interval. If the Hα emission disappears at about phase $+0.7$ (as implied by Joy's observations of Hγ, 1947), the dissipation of the shock energy is strong and rapid. Other observations are necessary to confirm this sudden weakening.

Comparison with the infrared shock model of Hinkle et al. (1982) shows that two shocks of large amplitude (i.e., ionizing hydrogen) are simultaneously present in the atmosphere at about luminosity minimum. Willson et al. (1982) also propose that there are two shocks, but at about luminosity maximum. In the case of Mira, the upper shock would be of small amplitude, i.e. would not produce Hα in emission.

Acknowledgements. We are grateful to Drs. M. O. Mennessier and A. Figer for magnitude estimates of Mira by the AFOEV and GEOS groups, respectively, and in particular to Dr. B. Barbuy for taking the spectra at phase $+0.27$. We also thank Dr. J. G. Phillips for his list of TiO wavelengths and Drs. C. I. Björnsson, J. P. J. Lafon, L. B. Lucy, and R. Svensson for relevant discussions.

References

Bonneau, D., Foy, R., Blazit, A., Labeyrie, A.: 1982, *Astron. Astrophys.* **106**, 235
Deutsch, A.J., Merrill, P.W.: 1959, *Astrophys. J.* **130**, 570
Enard, D.: 1982, *Proceedings of* SPIE **331**, 232
Gillet, D., Lafon, J.P.J.: 1983, *Astron. Astrophys.* (in press)
Gorbatskii, V.G.: 1961, *Soviet Astron.* **5**, 192
Hill, S.J., Willson, L.A.: 1979, *Astrophys. J.* **229**, 1029
Hinkle, K.H., Barnes, T.G.: 1979, *Astrophys. J.* **227**, 923
Hinkle, K.H., Hall, D.N.B., Ridgway, S.T.: 1982, *Astrophys. J.* **252**, 697
Joy, A.H.: 1947, *Astrophys. J.* **106**, 288
Joy, A.H.: 1954, *Astrophys. J. Suppl.* **1**, 39
Maehara, H.: 1968, *Publ. Astron. Soc. Japan* **20**, 77
Merrill, P.W.: 1955, *Publ. Astron. Soc. Pacific* **67**, 199
Merrill, P.W.: 1960, in *Stars and Stellar Systems* **6**, Chap. 13, ed. J.L. Greenstein, Univ. Chicago Press
Mihalas, D.: 1978, *Stellar Atmosphere*, second edn., Sect. 14-2, Freeman, San Francisco
Phillips, J.G.: 1983 (private communication)
Pierce, J.N., Willson, L.A., Beavers, W.I.: 1979, *Publ. Astron. Soc. Pacific* **91**, 372
Rowan-Robinson, M., Harris, S.: 1983, *Monthly Notices Roy. Astron. Soc.* **202**, 767
Stumpff, P.: 1980, *Astron. Astrophys. Suppl.* **41**, 1
Tsuji, T.: 1971, *Publ. Astron. Soc. Japan* **23**, 275
Wagenblast, R., Bertout, C., Bastian, U.: 1983, *Astron. Astrophys.* **120**, 6
Whitham, G.B.: 1958, *J. Fluid Mech.* **4**, 337
Willson, L.A.: 1976, *Astrophys. J.* **205**, 172
Willson, L.A., Hill, S.J.: 1979, *Astrophys. J.* **228**, 854
Willson, L.A., Wallerstein, G., Pilachowski, C.A.: 1982, *Monthly Notices Roy. Astron. Soc.* **198**, 483
Wood, P.R.: 1979, *Astrophys. J.* **227**, 220
Zel'dovich, Ya. B., Raizer, Yu. P.: 1966, Physics of Shock Waves and High-Temperature Hydrodynamic Phenomena, Vol. 1, Sect. III-9, Academic Press, London, New York